ELSEVIER

Journal of Structural Geology 29 (2007) 664–680

JOURNAL OF STRUCTURAL GEOLOGY

www.elsevier.com/locate/jsg

Late Quaternary kinematics, slip-rate and segmentation of a major Cordillera-parallel transcurrent fault: The Cayambe-Afiladores-Sibundoy system, NW South America

A. Tibaldi [a,*], A. Rovida [b], C. Corazzato [a]

[a] *Dipartimento di Scienze Geologiche e Geotecnologie, Università di Milano-Bicocca, Milano, Italy*
[b] *Istituto Nazionale di Geofisica e Vulcanologia, sezione di Milano, Milano, Italy*

Received 21 April 2006; received in revised form 28 November 2006; accepted 28 November 2006
Available online 2 February 2007

Abstract

We describe the recent activity of the Cayambe-Afiladores-Sibundoy Fault (CASF) and recognise it as one of the major potential active structures of northwestern South America, based on field observations, stereoscopic aerial photos of offset late Pleistocene-Holocene deposits and landforms, and crustal seismic activity. The CASF runs for at least 270 km along the sub-Andean zone of northern Ecuador and southern Colombia. We measured systematic latest Pleistocene-Holocene right-lateral strike-slip motion and right-lateral reverse motion consistent with earthquake focal mechanism solutions, and estimated a 7.7 ± 0.4 to 11.9 ± 0.7 mm/yr slip-rate. Magnitudes of the earthquakes that could be generated by possible fault-segment reactivation range up to **M** 7.0 ± 0.1. The CASF should be considered as a major source of possible future large magnitude earthquakes, presenting a seismic hazard for the densely populated regions to the west. The CASF is part of the tectonic boundary of the North Andean block escaping NNE-wards with respect to the stable South American plate.

Keywords: Ecuador; Colombia; Active fault; Seismicity; Slip-rate calculation

1. Introduction

The Andes of Venezuela, Colombia and north-central Ecuador behave as a microplate, the North Andean Block, which has been moving NNE-wards with respect to the more stable South American plate since at least the late Pleistocene-Holocene (Tibaldi and Ferrari, 1992) to the Present (Kellogg and Vega, 1995; Trenkamp et al., 2002). Based on seismic data, Pennington (1981) placed the eastern boundary of this microplate with the South American plate along a right-lateral strike-slip fault zone from the Guayaquil Gulf in Ecuador to the northern Venezuela coast (Fig. 1). More recent neotectonic field data and analyses of local seismicity depict a more complex fragmentation of the North Andean Block, represented by Holocene and active motion along nearly parallel transcurrent and reverse faults that partition the deformation (Ferrari and Tibaldi, 1992; Balseca et al., 1993; Paris and Romero, 1993; Chorowicz et al., 1996; Ego et al., 1996; Taboada et al., 2000; Tibaldi and Romero, 2000). These recent discoveries suggest new potential seismogenic faults. Recognising the major seismogenic faults and their features is fundamental for seismic hazard, and risk assessment and management. In the Andes of northern Ecuador and southern Colombia, it is unclear which are the major active faults despite the occurrence of large seismic events.

Using new geological-structural field data on offset late Pleistocene-Holocene geomorphic features and deposits, seismic data on distribution of crustal earthquakes and related focal mechanisms, and interpretation of stereoscopic aerial photos, we describe the latest Pleistocene-Holocene activity of the Cayambe-Afiladores-Sibundoy Fault (CASF), which allows us to recognise it as a potential major active structure of

* Corresponding author. Dipartimento di Scienze Geologiche e Geotecnologie, P. della Scienza 4, 20126 MILANO, Italy. Tel.: +39 02 6448 2052; fax: 39 02 6448 2073
E-mail address: alessandro.tibaldi@unimib.it (A. Tibaldi).

0191-8141/$ - see front matter © 2006 Elsevier Ltd. All rights reserved.
doi:10.1016/j.jsg.2006.11.008

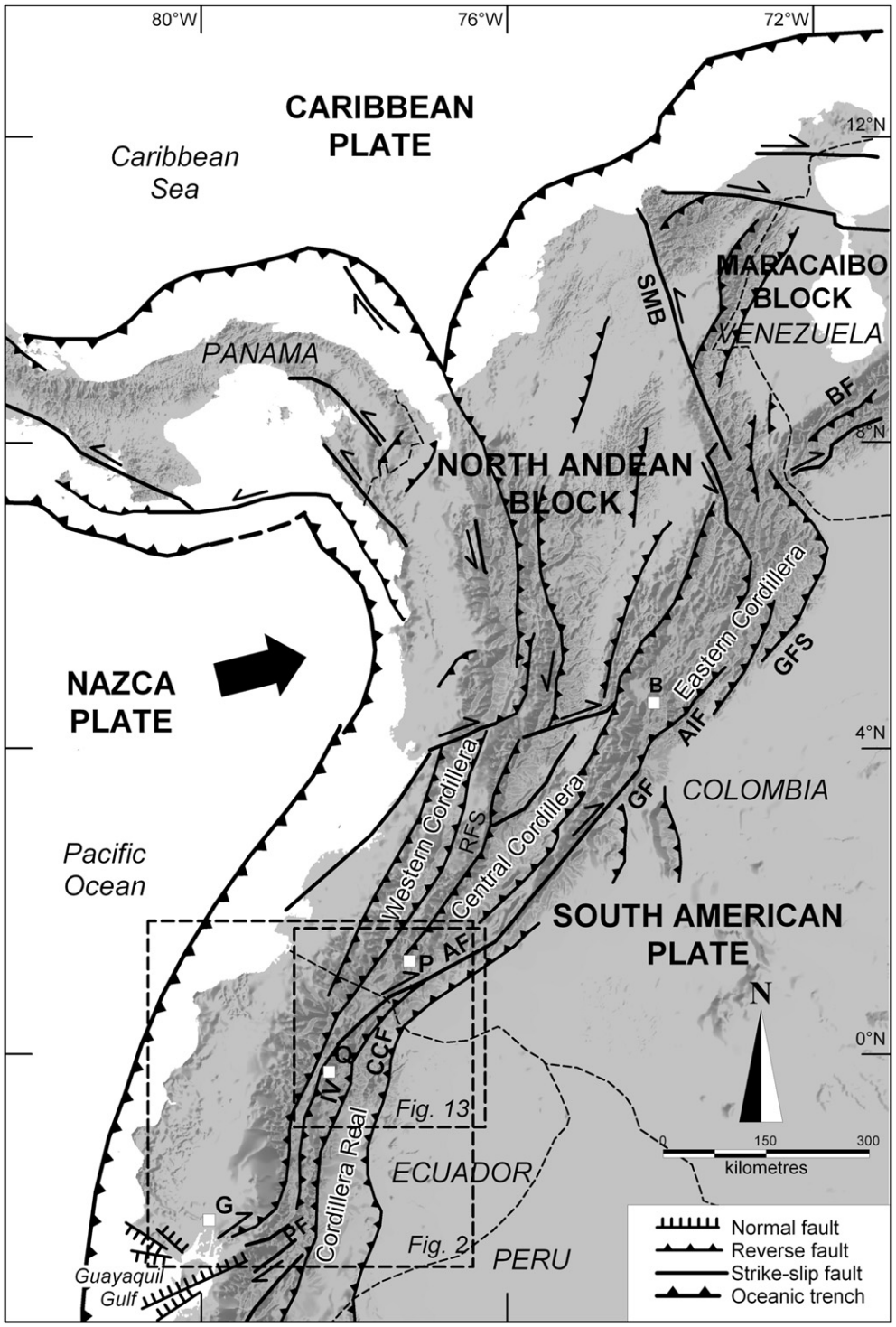

Fig. 1. Plio-Quaternary tectonic framework of the North Andean Block. Fault traces are from Pennington (1981), Tibaldi and Ferrari (1992), Ego et al. (1996) and Taboada et al. (2000). PF = Pallatanga Fault, IV = Interandean Valley, CCF = Cayambe-Chingual Fault, AF = Afiladores Fault, RFS = Romeral Fault System, GF = Garzon Fault, AIF = Algeciras Fault, GFS = Guaicaramo Fault System, BF = Boconò Fault, SMB = Santa Marta-Bucaramanga Fault; G = Guayaquil, Q = Quito, P = Pasto, B = Bogotà. Boxes show locations of Figs. 2 and 13.

northern Ecuador and southern Colombia. Some evidence of late Quaternary activity of the Colombian part of this structure was given by Tibaldi and Romero (2000), whereas Velandia et al. (2005) used satellite image interpretations. In this paper we recognize the recent/active fault traces that suggest a segmentation of the CASF. This result is of international interest because the CASF represents part of the eastern main tectonic boundary of the northern Andes. Our conclusions can be compared with studies in neighbouring regions. This work also provides two methodological contributions: first, it describes how fault slip-rates can be reconstructed in a region where geological and environment characteristics do not allow

classical radiometric dating of offset deposits. We instead used systematic age estimation of the landforms cut by the fault segments based on regional/global changes with local calibration points, as a first-order control on the morphological evolution. As a second methodological contribution, we used systematic morphometric analyses along the entire length of the structures. In this way, we calculated the slip-rates related to different time spans (different ages of offset landforms and deposits) and the slip-rates for the same time span but in different fault segments of the structure and at different points of the same segment. This approach allows better constraints on the kinematics and behaviour of a fault.

2. Geological background and tectonic setting

Two geographically and geologically different regions characterise the NW part of South America: the flat and stable Amazonian shield to the east and the active and deformed mountainous Andean area to the west, associated with the eastward subduction of the Nazca oceanic plate beneath the South American continental plate. In Ecuador (at about 2°S) the Andes divide into two parallel chains, the Western Cordillera and the Cordillera Real, separated by the Interandean Valley. In Colombia the Andes divide into three ranges, the Western, Central and Eastern Cordilleras (Fig. 1).

In Ecuador and Colombia (Fig. 2), the Western Cordillera is mainly composed of a Cretaceous-Eocene sequence of igneous and marine sedimentary rocks (Henderson, 1979; Lebrat et al., 1987; Gonzalez et al., 1988) accreted to the South American continental margin during the Early Tertiary (Feininger and Bristow, 1980; Roperch et al., 1987; Litherland and Aspden, 1992). The fault systems of the Interandean Valley in Ecuador and of the Cauca-Patia Valley in Colombia (Romeral Fault System, Fig. 1) follow a Late Cretaceous-Early Tertiary suture

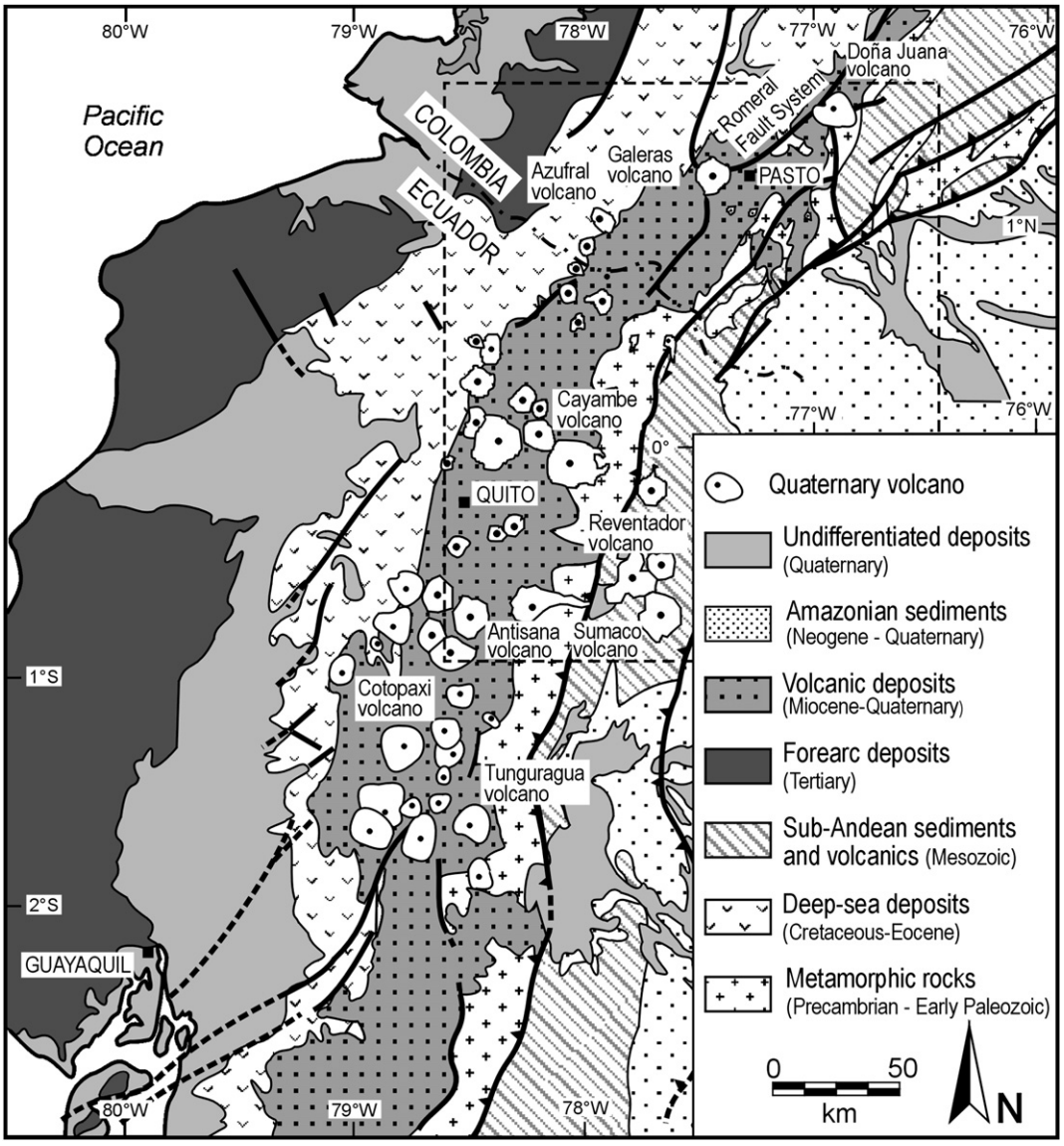

Fig. 2. Geological sketch-map of Northern Ecuador and Southern Colombia, from this study, Barberi et al. (1988), INGEOMINAS (1988), Wallrabe-Adams (1990) and Tibaldi and Ferrari (1992). Map location is shown in Fig. 1. Box shows location of Fig. 3.

between an island arc and the continental paleomargin (Litherland and Aspden, 1992).

The Cordillera Real in Ecuador and the Central Cordillera in Colombia (Fig. 1) are part of a metamorphic belt that runs continuously from the Caribbean coast of Colombia and Venezuela to the Peruvian border (DGGM, 1986; Gonzalez et al., 1988) (Fig. 2). The Eastern Cordillera of Colombia is a NNE trending intracontinental belt made up of Precambrian-Palaeozoic metamorphic rocks and Mesozoic-Cenozoic deformed sedimentary rocks (review in Taboada et al., 2000).

The Sub-Andean Zone represents the connection between the high Andean ranges and the Amazonian lowland. It mainly comprises volcanic and sedimentary rocks (Fig. 2) thickening eastward and covering the metamorphic basement of the Precambrian Guayana Shield (Feininger and Bristow, 1980; Gonzalez et al., 1988).

3. The Cayambe-Afiladores-Sibundoy fault

3.1. Structural framework

The Ecuadorian segment of the CASF, and its Quaternary activity, was first described by Ferrari and Tibaldi (1989) and Tibaldi and Ferrari (1992) as the Cayambe-Chingual fault and then by Ego et al. (1996) as the Cayambe-La Sofia fault. Our data show that the CASF continues for at least 270 km along the sub-Andean zone of northern Ecuador and southern Colombia (Fig. 3). Its surface expression is represented by one or more parallel fault traces striking NNE to NE. Several faults with these strikes have been mapped in the north-eastern Andes and with local names such as Algeciras, Suaza, Garzon, Pitalito and Altamira, but only a few have been identified with neotectonic activity. Among the latter we have the Afiladores

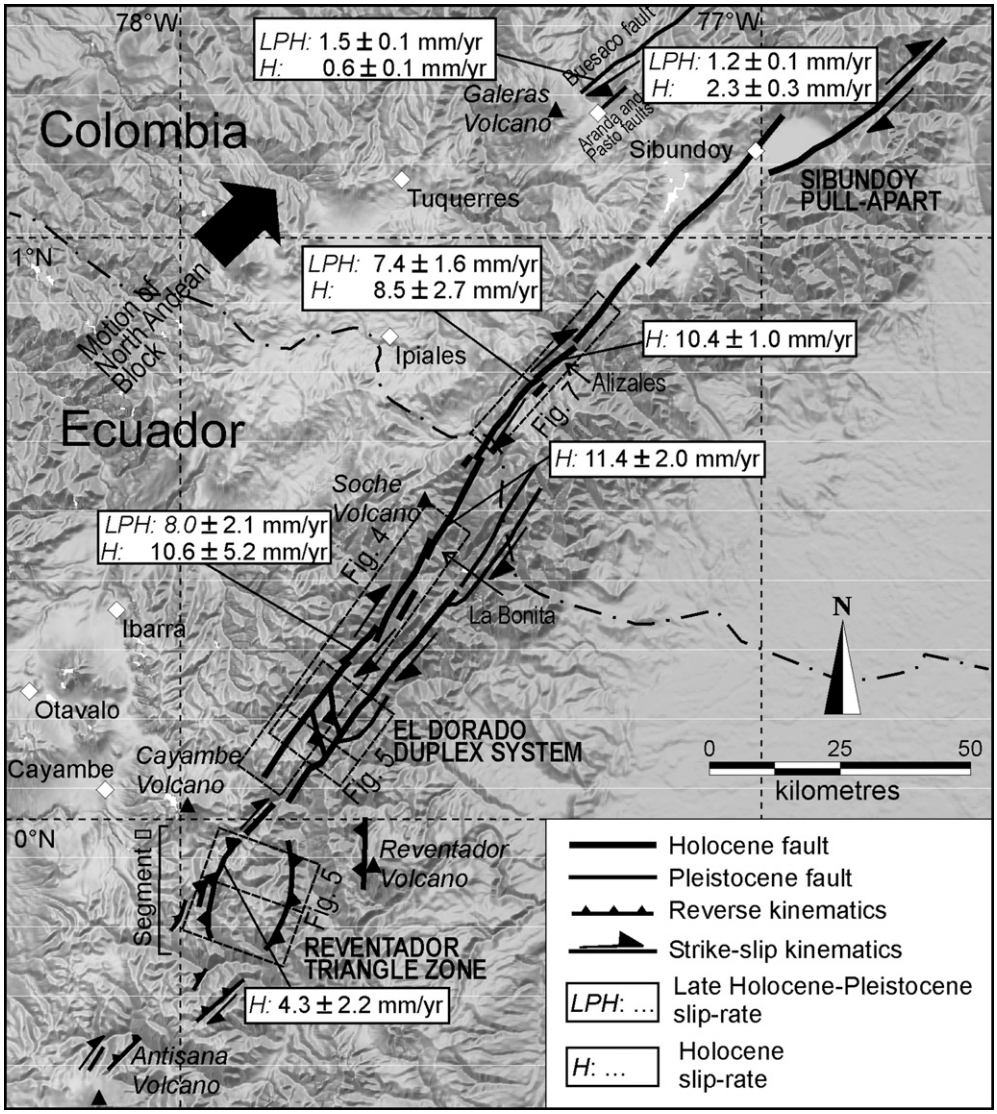

Fig. 3. Main tectonic features along the Cayambe-Afiladores-Sibundoy fault. Slip-rates are from measurements of dated offset geologic deposits and landforms for two different time spans: late Pleistocene-Holocene and Holocene. Buesaco, Aranda and Pasto faults are from Tibaldi and Romero (2000) and Rovida and Tibaldi (2005). Map location is shown in Fig. 2.

Fault (Paris and Romero, 1993) north of the Ecuadorian border, the Garzon Fault in Southern Colombia (Chorowicz et al., 1996), the Algeciras Fault in Central Colombia (Paris and Romero, 1993), the Guaicaramo Fault System in Northern Colombia (INGEOMINAS, 1998) and the Bocono Fault in Venezuela (Schubert, 1980).

The segments of the CASF that we classified as bearing evidence of recent/active tectonics, usually offset valleys and crests trending NW-SE orthogonal to the fault trace. Locally, the CASF trace coincides with valley floors trending NE-SW or runs along the valley slopes. In this case fresh uphill-or downhill-facing scarps were used as neotectonic indicators. We stress that only field investigations and interpretation of aerial stereoscopic photos allowed us to appreciate this three-dimensional evidence of neotectonic activity. Following offset Quaternary landforms and deposits, we found discontinuities and step-overs along the main fault trace. We ignored fault lineaments from satellite images or geological maps with no evidence of recent motion. We classified segments of the CASF based on degree of erosion, continuity, consistency of orientation and kinematics. These segments will be described in detail in the following sections, starting from the southern part of the CASF in Ecuador.

3.2. Structure and segmentation of the southern part (Ecuador)

Here we recognized four main segments (Figs. 3 and 4). The southern termination of the CASF (segment I, Fig. 3) is characterised by a splay opening southward. Here, mountain crests, river channels, glacial circles and valleys are offset by NNE- and N-S-striking faults. Due to the high altitude of the area and to the characteristics of the moraines in the area (unlitified, no alteration of pebbles, uppermost stratigraphic position, poor soil development, freshness of the glacial abrasion surfaces, etc.), the glacial landforms have been dated to the Last Glacial Maximum (LGM) of late Pleistocene age (Thouret et al., 1997). The NNE-striking faults dominate between Cayambe and Antisana volcanoes and limit blocks whose major movements are right-lateral strike-slip. The vertical planes of the faults in the field, as well as their rectilinear trace in plan view across rugged topography, indicate a vertical dip. The N-S striking faults limit blocks with dominant vertical movements. The two main N-S faults, to the southeast of the Cayambe volcano, are about 15 km long and face each other with dips in the order of 70–80°, creating a "triangle zone structure" (McClay, 1992) (Fig. 5C). As a whole, this southern termination of the CASF can be defined as a leading contractional fan according to the terminology of Woodcock and Fischer (1986), followed to the northeast by a restraining bend (Figs. 3 and 5).

Further northeast, at the latitude of Cayambe Volcano, the fault traces are highly segmented, strike NNE and NE and show right-lateral strike-slip to locally reverse right-lateral motion (Fig. 4A). Northeast of Cayambe Volcano, a NE-striking rectilinear fault trace runs continuously for 14 km (segment II, Figs. 4 and 6). West of its NE termination, another fault runs with the same direction for about 13 km to Rio Cofanes, where it bends from NE to ENE and connects to another fault. This is a rectilinear right-lateral strike-slip fault extending for 37 km (segment III, Figs. 4 and 6). At the northeastern termination of segment III, another NE-striking fault starts with a right-lateral step-over (segment IV). This fault runs for 15 km across the Colombia border, together with two other minor parallel surface ruptures (Fig. 7). Outcropping fault planes (Fig. 4B) and the rectilinear fault trace in plan view across rugged topography indicates nearly vertical dips for all these structures.

Rivers, crests and deposits show systematic right-lateral displacements and a minor component of vertical motion resulting in an uplift of the NW tectonic block. A lava flow of the Soche Volcano dated 9.7 ka BP by Hall and Beate (1991) was displaced (Fig. 8). Aligned landslides and triangular facets are also present along the structure.

3.3. Structure and segmentation of the central-northern part (Colombia)

In Colombia, along the Afiladores river, a recent fault presents a single clear surface trace (segment V) that runs almost rectilinearly up to 17 km NE of the Ecuador-Colombia border (Fig. 7). Further NE another single and clear surface trace (segment VI, Fig. 7) starts with a left-lateral step-over and continues for 12 km up to Alizales village. In the step-over area another 5-km-long fault trace is present on the opposite side of the valley. Along these fault traces, hillcrests, rivers and gullies show clear right-lateral offsets and locally a slight vertical component with uplift of the NW tectonic block. Field data shows that these faults have a vertical dip (Fig. 9).

We observed in the field systematic evidence of asymmetric development of approximately NW-SE-trending valleys dislocated by the CASF (Figs. 10 and 11). The segments of these valleys located southeast of the fault (i.e. lower channels) show a gently inclined slope on the southwestern valley side and a steep slope on the opposite valley side (i.e. to the northeast). The southwestern slopes gradually connect to the valley floor where several levels of fluvial terraces and deposits occurred. Between these deposits and the upper part of the slopes we found debris talus (Fig. 11). The northeastern slopes abruptly connected to the valley floors where the active streams is usually located. These slopes are frequently affected by small landslides. In the valley segments located northwest of the CASF (i.e. upper channels) we observed the same characteristics but with an inverted geometry, i.e. gentle slopes on the northeast side of the valley and steep slopes on the southwest side (Fig. 10). We explain this topography as the effect of river erosion and deposition during migration of the stream to restore the original geometry diverted by right-lateral faulting. Near the fault, the river migrated southwestward on the NW tectonic blocks, and northeastward on the SE blocks. The asymmetric valleys developed near the fault trace, whereas the valleys are symmetric in cross-section farther away from the fault trace.

Immediately northeast of Alizales, the fault bends to a NNE strike for about 17 km and then re-attains its NE strike (Fig. 3). The main fault trace is visible for another 42 km to the

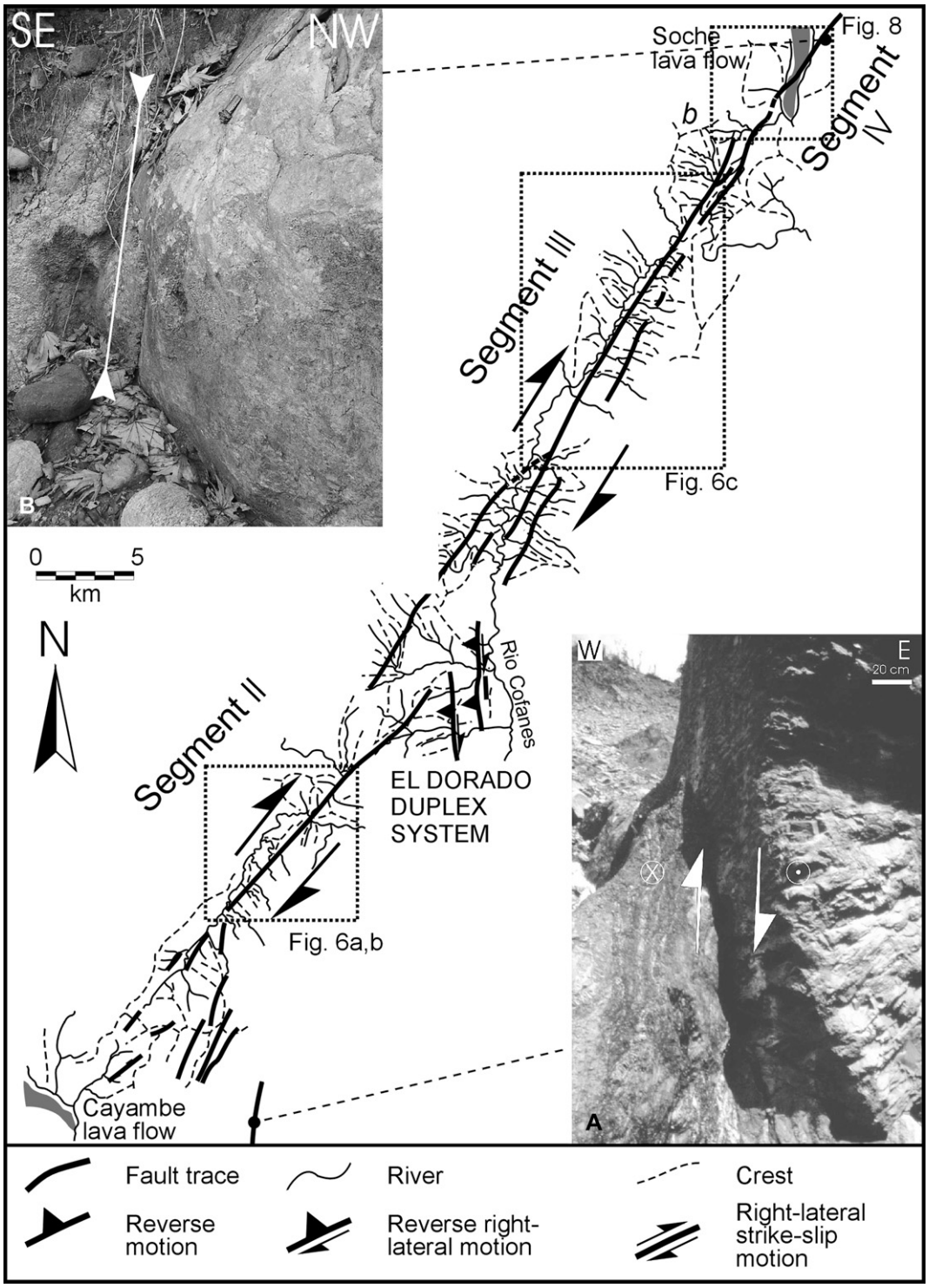

Fig. 4. General geometry and features of the southern part of the CASF (Ecuador). At bottom left the segmentation of the CASF NE of the Cayambe Volcano is clear. Further NE the fault becomes a single trace (segment II) and then steps 2.5 km NW-ward, to connect to segment III on the opposite side of the Rio Cofanes valley. Segment III is one long single trace, paralleled by four minor traces. At top right the Soche lava flow offset by segment IV is shown. *A*. Holocene, NNE-striking reverse-right-lateral oblique fault. *B*. Outcropping fault plane showing the near vertical dip. Boxes show the areas enlarged in Figs. 6a,b,c and 8. Map location is shown in Fig. 3.

Sibundoy Valley (segment VII), where a more complex structure occurs. Here the fault splits into two parallel NE-striking segments with a right-stepping arrangement, consistent with a right-lateral pull-apart model. Further evidence of Holocene and very recent motion include: main fault scarps have triangular facets and displace rivers, gullies and alluvial fans, while tilting of recent deposits is present near the valley floor and at the base of the fault scarps.

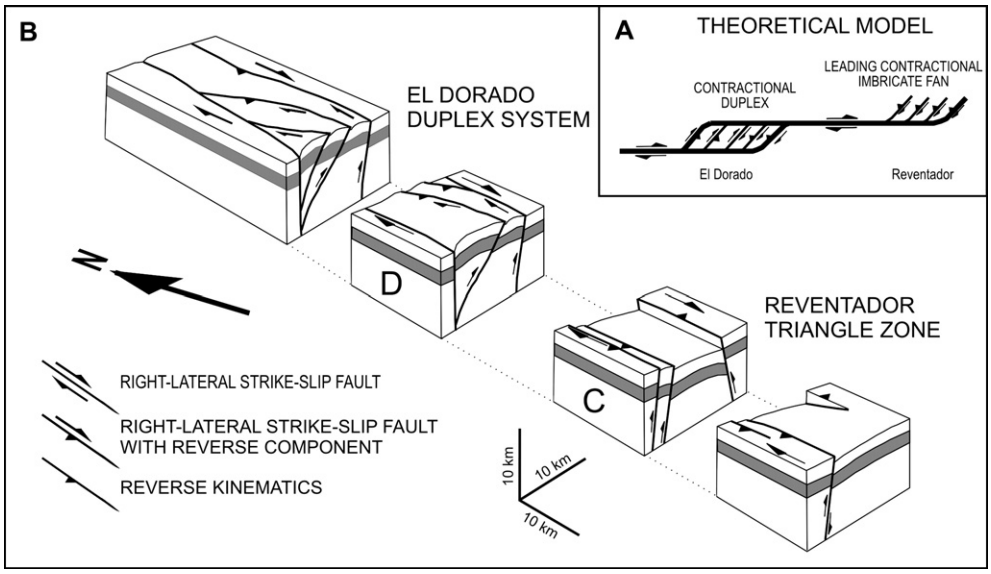

Fig. 5. The southern termination of the right-lateral CASF can be described as a leading contractional fan according to the terminology of Woodcock and Fischer (1986), followed to the NE by a contractional duplex (El Dorado Duplex System). The structure SE of Reventador Volcano can be described as a ''triangle zone structure''. *D* and *C* are structures located in Fig. 3.

4. Fault slip-rate calculation

4.1. Methodology

Slip-rates can be used to evaluate the activity of a fault segment. To better constrain the kinematics of the CASF, we calculated the slip-rates related to different time spans (different ages of offset landforms and deposits). Moreover, slip-rate was computed for the same time span also in different segments of the fault system and with multiple measurements along each segment. We also measured dated offset landforms with calibration points based on dated offset deposits. These methods can be useful in areas where collecting samples for classical absolute dating such as radiocarbon is difficult or impossible. The time span involved in the studied fault motions is larger that the last 40 ka range of ^{14}C. Moreover, outcrops showing faulted buried palesoils that can be dated are extremely rare and artificial trenching along this fault is almost impossible due to its remote location. Tropical highly-humid weather of these regions can also affect ^{14}C dating.

Regarding the number of measurements, several previous papers defined the slip-rate of a fault by a single measurement, although slip-rates can change along the same fault trace within a given time span. Actually, apart from the age of the involved deposits and the repetitive reactivation of a fault segment, surface offset can also vary due to a change from concentrated to distributed deformation, from faulting to folding (McCalpin, 1996) and due to the influence of topography (Tibaldi, 1998; Strom, 1999), or from changes in rock rheology (Groppelli and Tibaldi, 1999). Thus, in view of the great length of the studied structure, we collected several measurements of coeval offset landforms in different segments of the fault.

Measurement of offset deposits gives a fault finite cumulative displacement. The same type of displacement value can be obtained from offset fossil landforms, such as glacial valleys, cirques, moraines and alluvial fans. Offsets of active river valleys should be used more carefully, mainly due to the typical morphological evolution of river channels: they can abandon their offset lower channel to spill spontaneously over the fault zone and cut a new channel below the fault zone (Wallace, 1968). This river reorganisation can develop into an alignment of upstream and downstream segments of former parallel channels, leading to a connection between channels across the fault trace with no apparent offset. Alternatively, downstream channels of adjacent rivers can capture the upstream channel (Gaudemer et al., 1989), leading to a connection between an upstream segment and the downstream segment of its neighbour and suggesting an apparent offset opposite to the sense of motion of the fault. All this is strongly influenced by the characteristic spacing of rivers, which in turn is a function of the hydrology and lithology of the area (Gaudemer et al., 1989). Once we established a right-lateral sense of motion for the CASF with unequivocal indicators, such as an offset lava flow and other fossil landforms, we retrodeformed the observed features to evaluate their true displacement. In areas with the same lithology and hydrology, river lengths and valley widths grow with time. Gaudemer et al. (1989) observed that along several active strike-slip faults river offsets vary suggesting that rivers may respond differently to the perturbation of their geometry by faulting, depending on the age of the valley. Thus, in this paper measurements of river offsets have been statistically divided into homogeneous sets based on the ratio between river length-valley width and offset amount.

4.2. From ages of offset landforms and deposits to fault slip-rates

Absolute dating of faulted deposits is available for lavas of Soche and Reventador volcanoes (see Table 1). Most of the slip-rate computations are based on the estimated age of the

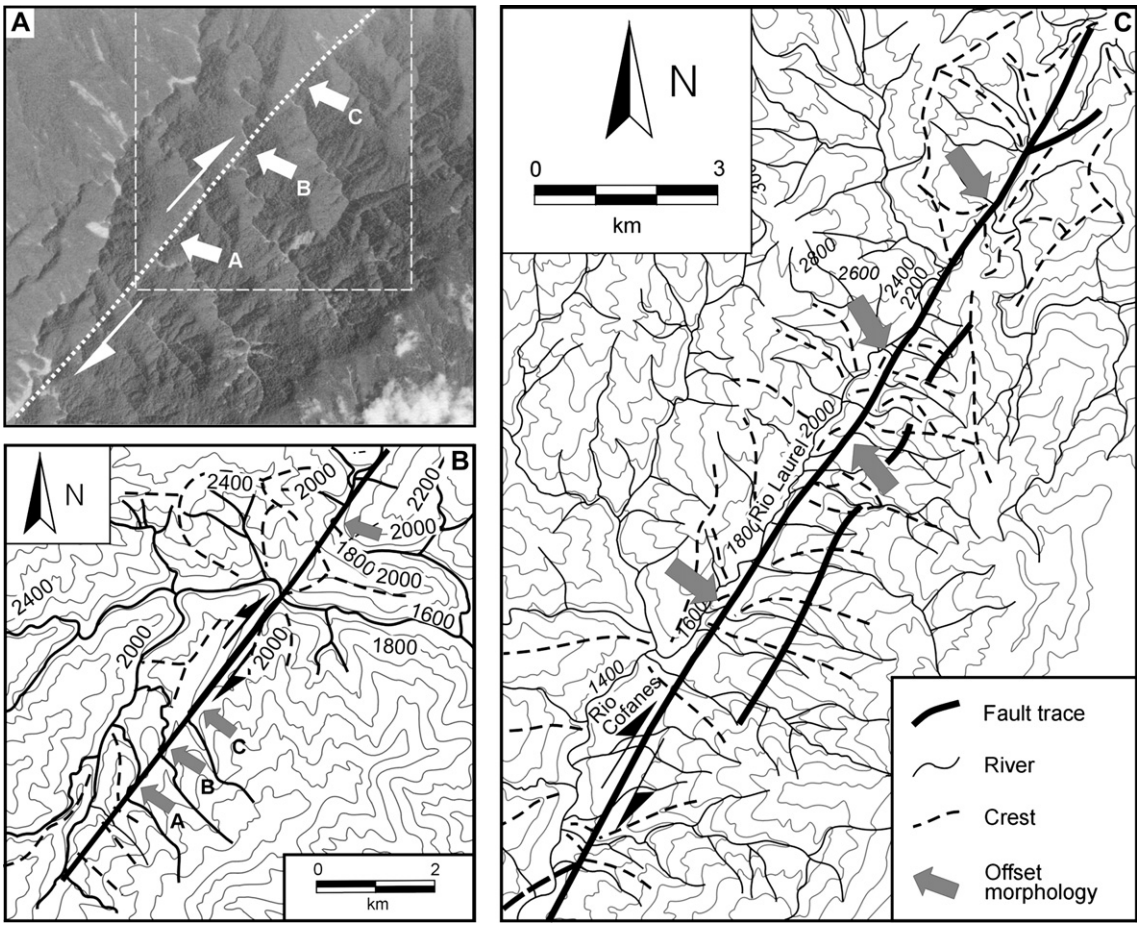

Fig. 6. Right lateral displacement of geomorphic features along Segments II (A and B) and III (C). Location is shown in Fig. 4.

glacial or fluvial morphologies cut by the fault segments. At altitudes lower than the past glacial environment, Montgomery et al. (2001) show that the morphology of the Northern Andes is dominated by fluvial erosion. They suggest climate variations as a first-order control on the morphological evolution of the entire range. Taking into account the morphological features and the latitude and altitude of the studied area, we interpreted the periods of inferred humid tropical climate and of major fluvial erosion as the intervals during which the development of the present drainage pattern occurred. These are compared with the ages of the glacial fluctuations in the Andes.

Iriondo (1999) identifies three different climatic patterns that occurred at a continental scale in South America during the Late Quaternary. In the Andes of Ecuador and Southern Colombia a climatic pattern similar to the one recognised in the Pampean Sand Sea (PSS) of Argentina (''Pampean pattern'') has been described. The PSS climatic record starts at Isotopic Stage 4 (ca. 73–59 ka BP; Martinson et al., 1987) and shows a very cold climate over the whole of South America with glacial advances in the Andes during this interval. The beginning of this cold interval is also represented by the pollen record of the plain of Bogotà (Colombia) that indicates a decrease in temperature at the boundary between Bacatanian and Fuquenian chronostratigraphic units (Van der Hammen and Hooghiemstra, 1997), with an age of 73 ka BP. In the PSS record, the Isotopic Stage 3 (ca. 59–24 ka BP; Martinson et al., 1987) is marked by a climatic warming with three events: I) a rapid climatic change to humid tropical conditions and high precipitation that lasted about 4–5 ka; II) a semiarid climate; and III) a second humid phase with precipitation higher than at present (Iriondo, 1999). During these periods important fluvial belts developed and fluvial sediments related to this interval gave a TL date of 45.6 ± 2 ka BP (Iriondo, 1999). A humid and warm climate between 42 and 36 ka BP was also deduced from a pollen record (Heusser, 1974). Moreover a glacial interstadial was recognized in the Cordillera Central of Colombia between ca. 34 and 27 ka BP (Thouret et al., 1997). Isotopic Stage 2 (ca. 24–12 ka BP; Martinson et al., 1987) is characterized by an arid climate in the lowlands and by a generalized advance of glaciers in the Andes (Iriondo, 1999). This period corresponds to the Last Glacial Maximum (LGM), during which glaciers reached their maximum extent in the Central Andes of Colombia with two glacial stades dated 28–21 ka BP and 21–14 ka BP (Thouret et al., 1997). Three glacial advances were also recognized in the Bogotà area and referred to the intervals 23.5–19.5, 18.0–15.5 and 13.5–12.5 ka BP respectively (Helmens et al., 1997). During Isotope Stage 2 a climatic warming occurred about 15–16 ka BP, when the climate became humid enough

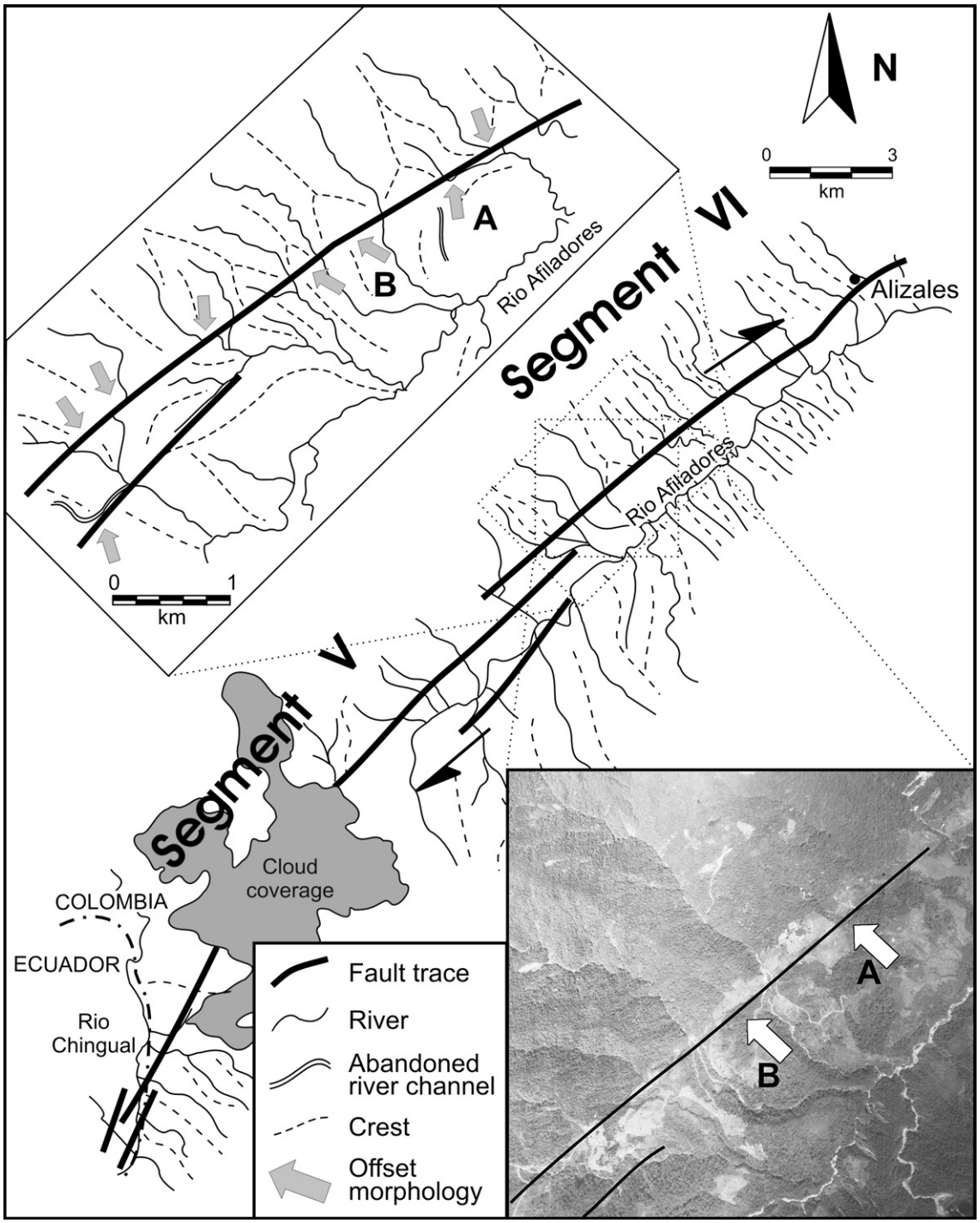

Fig. 7. Geometry and features of the central part of the CASF (Colombia, located in Fig. 3), as observed on a Landsat TM image and aerial stereoscopic photos and field checked. Note the single marked surface trace on the NW side of the Rio Afiladores valley and the step-over geometry between segments V and VI. Position of measured offset landforms is shown in the enlarged area, where the right-lateral sense of motion can be seen, despite the presence of some captured and abandoned river channels.

to favour pedogenic processes (Iriondo, 1999). This climatic warming was also observed in Chile between 17 and 14 ka BP (Heusser, 1974). The PSS record indicates a prevailing cold and dry climate in the interval 14–8.5 ka while a climatic cooling with widespread active fluvial erosion characterizes the early Holocene from 8.5 to 3.5 ka BP (Iriondo, 1999).

The fluvial morphological features offset by the CASF developed in the intervals characterized by humid, warm climates. Based on these climatic reconstructions and considering the age of the Soche lava flow as an ''anchor-point'' for slip-rates, we concluded that the larger offsets measured along the fault may have been produced during the second humid phase of IS 3, before 40 ka BP, when a period of reduced fluvial

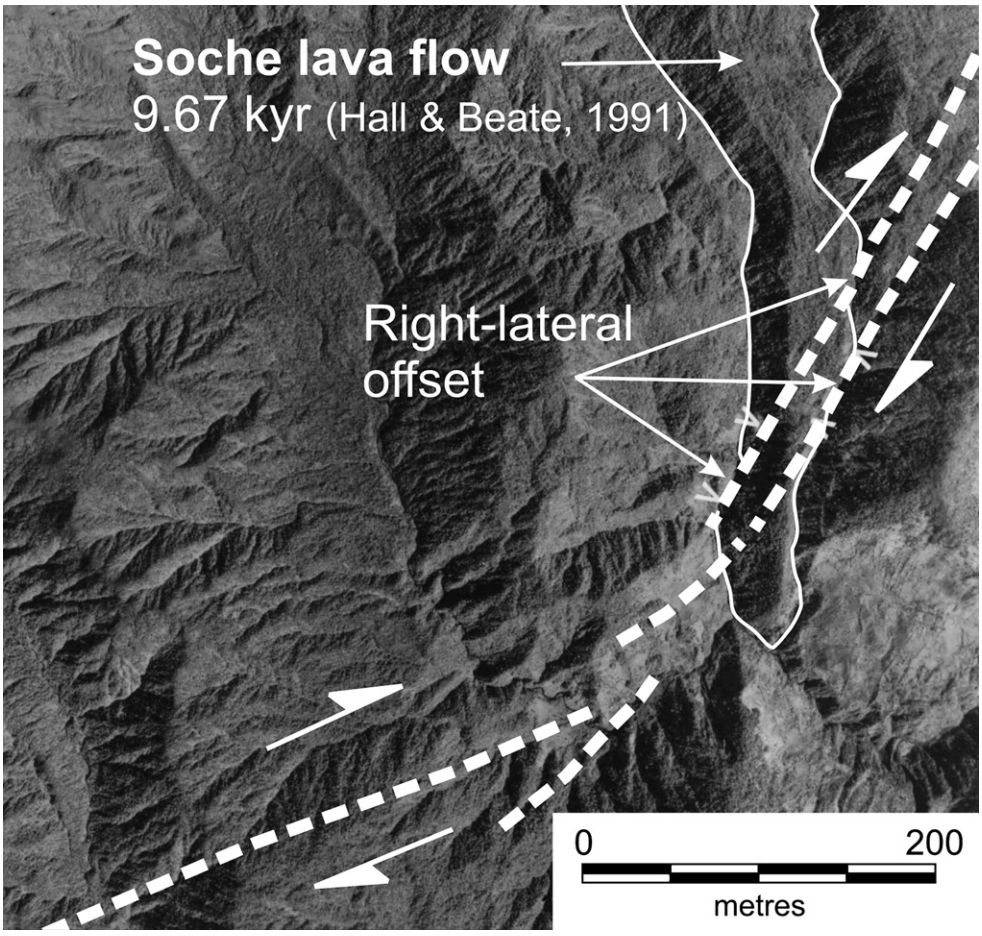

Fig. 8. Aerial view of the right-lateral strike-slip offset of the Soche Volcano lava flow. Note that the total cumulated slip here was produced by motions on a series of parallel fault planes.

discharge observed for the Peruvian Amazon rivers started (Dumont et al., 1992). As the beginning of this interval is not determined we assumed the climatic warming indicated by fluvial sediments dated 46 ka as a maximum age. The next main morphogenetic phase occurred after the period of reduced fluvial discharge, i.e. after 32 ka (Dumont et al., 1992) and before the end of the glacial interstadial recognized in the Colombian Andes between 34 and 27 ka BP (Thouret et al., 1997). The last phase considered is between the climatic warming at 16 ka BP and the beginning of the following dry phase at 14 ka BP (Iriondo, 1999).

Starting from the SW termination of the CASF in Ecuador (segment I), we measured the dislocation of glacial landforms, which, due to the altitude of the area and to the freshness of the morphologies, can be related to the LGM aged 28–14 ka (Thouret at al., 1997). Here N-S-striking reverse faults show 30 ± 5 m, 20 ± 5 m, and 25 ± 5 m of vertical motion, which corresponds to slip-rates of 1.7 ± 0.8, 1.2 ± 0.6 and 1.4 ± 0.7 mm/yr respectively, totalling 4.3 ± 2.2 mm/yr along the three parallel faults. Several measurements of river and hillcrest offsets were also collected along the CASF segments II and III, located NE of the Cayambe Volcano (Fig. 4). The average right-lateral offset of the larger gullies is 285 ± 70 m which

Fig. 9. Photo of fault planes belonging to the CASF system. The vertical rock wall cuts the faults so that they appear in section view, highlighted by the white arrows. The vertical dip of the faults can be observed. This outcrop is located near the Colombia-Ecuador border.

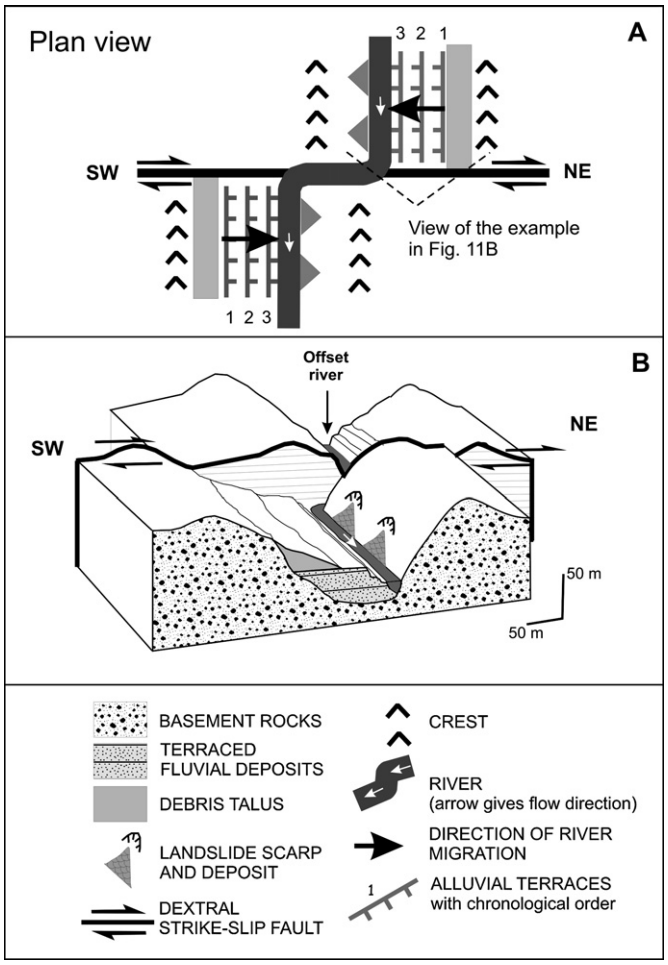

Fig. 10. Plan view and block diagram of the asymmetry observed for several NW-SE trending valleys at a short distance from the CASF trace. Downstream of the fault trace the southwestern valley side has a gently dipping slope with several levels of fluvial terraces, while the opposite side is steeper and affected by some landslides. Upstream of the fault trace the geometry is inverted. This is probably due to river migration to re-establish its original geometry diverted by the right-lateral faulting. The photograph in Fig. 11B shows an example of this situation observed near Alizales in Colombia.

was correlated with the interval 32–27 ka BP (Fig. 12), giving a slip-rate of 8.9 ± 3.1 mm/yr. The average offset of smaller gullies, 180 ± 64 m, correlated with the interval 16–14 ka BP implies a slip rate of 12.3 ± 7.2 mm/yr.

The lava flow of Soche Volcano has a right-lateral offset of 110 ± 60 m. From its 9.67 ka BP age (Hall and Beate, 1991) we obtain a slip-rate of 11.4 ± 6.2 mm/yr for segment IV (Fig. 12). It is noteworthy that for the same lava flow Ego et al. (1996) obtained an age of 37.22 ± 0.63 ka BP and an age of 8.6 ± 0.06 ka BP for a lahar deposit, with offsets of 307 ± 37 m and 50 ± 14 m respectively (Fig. 12), although no indication of the measurement methodology is given. With these value these authors obtain slip-rates of 8 ± 2 mm/yr and 6 ± 2 mm/yr respectively.

In Colombia we measured on aerial photos several offsets of rivers and hillcrests about 8 km SE of Alizales village (segment VI, Fig. 7). Average right-lateral dislocations cluster into three groups, 132 ± 27, 233 ± 24 and 331 ± 29 m (Fig. 12). Correlating these offsets with the above mentioned warm and humid periods, i.e. 14–16 ka BP, 27–32 ka BP and 40–46 ka BP, we obtained right-lateral components of slip of 8.9 ± 3.4 mm/yr, 8.0 ± 2.1 mm/yr and 7.4 ± 1.6 mm/yr respectively. Near Alizales village we measured in the field a right-lateral strike-slip component of 131 ± 1.3 m, and an uplift of the NW block of 120 ± 20 m (Fig. 11). Using the same age estimation for landforms as in the previous measurement site for small gullies, we obtained a horizontal slip-rate of 8.8 ± 0.9 mm/yr.

Other measurements collected along the Ecuadorian segment of the CASF gave a mean of 630 ± 70 m. On the basis of the above mentioned climatic records, it appears that a warm period may have occurred before the cold Isotopic Stage 4, i.e. before 74 ka BP (Martinson et al., 1987). This is also supported by the decrease in temperature that marks the end of the Bacatanian chronostratigraphic unit (Van der Hammen and Hooghiemstra, 1997). Lacking older absolute ages for South America, a lower limit for this period may be the transition between Isotopic Substages 5a and 5b, placed on a global scale at 86 ka BP (Martinson et al., 1987). If we assume the 74–86 ka BP interval to be the age of the 630 ± 70 m offsets, we obtain a slip-rate of 8.0 ± 2.0 mm/yr, consistent with the rates obtained for smaller offsets along the structure.

5. Seismicity of the region

In NW South America Pennington (1981) identified five seismic regions, on the basis of earthquake focal mechanisms. This author identifies an alignment of shallow events along the eastern front of the Andes. The related focal mechanisms are predominantly right-lateral strike-slip or thrusting. One nodal plane is nearly parallel to the NE alignment of the epicentres and to the trend of the Andean range (Fig. 13).

In northern Ecuador a number of large historical earthquakes are reported by CERESIS (1985). Major events with epicentral MCS intensity $I \geq IX$ occurred in 1541, 1557, 1587, 1755, 1757, and 1868 AD. They are concentrated along the NNE-trending Interandean Valley and Cordillera Real. The western Andes (i.e. Western Cordillera) have lower levels of crustal tectonic activity (Barberi et al., 1988; Pasquaré et al., 1990). Correlation of past large earthquakes with active structures in the Interandean Valley is difficult because the prime candidate, the Quito fault system, is either a blind structure or is hidden by numerous landslides and colluvial deposits (Hibsch et al., 1997).

To the east, along the Andean margin, an alignment of crustal instrumental events with **M** between 4 and 6 is present. The epicentres of two large earthquakes were located along the CASF in Ecuador, near the southwestern end of the fault (Fig. 13). They occurred on March 5, 1987 with $M_S = 6.1$ and $M_S = 6.9$ respectively. The focal mechanisms show a dominant thrust motion with a right-lateral strike-slip component and E-W-trending P axis (USGS, 1987). Centroid Moment Tensor solutions for the same events (Dziewonski et al., 1988) show nearly pure thrust motion but similar P and T axes.

In southern Colombia several historical seismic events with intensity $I > VIII–IX$ have occurred over the last centuries

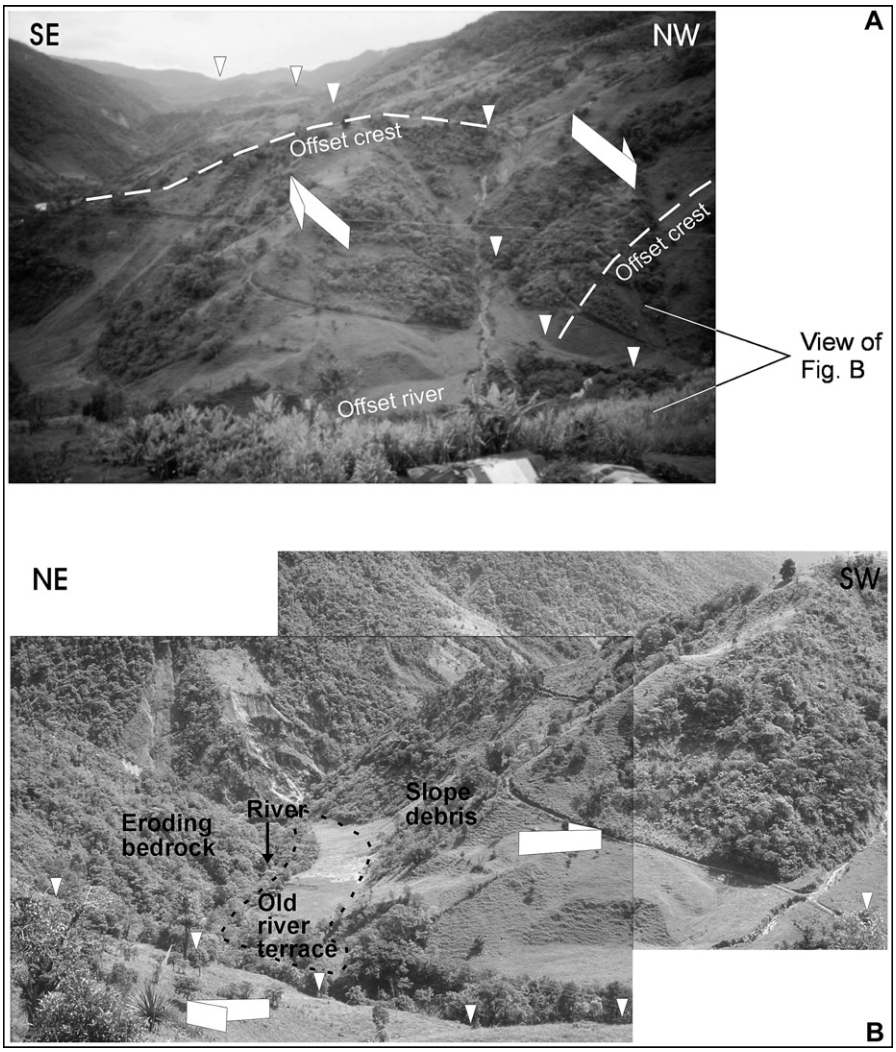

Fig. 11. (*A*) Photo of the CASF near Alizales village (Colombia), with offset crest and river. Triangles locate the fault trace. Measured displacement of the crest is 131 ± 1.3 m. (*B*) Photo of an asymmetric valley located NW of the CASF trace at Alizales. Triangles locate the fault trace. Note the development of river terraces and debris talus on the NE slope and the presence of a landslide on the steeper SW slope, as sketched in Fig. 10.

and were located in the Cauca and Magdalena interandean valleys (Ramirez, 1975; Escallon et al., 1993). Particularly large earthquakes affected the town of Pasto in 1696 AD (I > VII [Espinosa, 1994]), on January 20, 1834, between July 1935 and August 1936, and on July 14, 1974 (INGEOMINAS, 1995), causing casualties and severe destruction of buildings. The last large earthquake occurred on March 4, 1995, with local magnitude Ml = 5.1. Its hypocentre was placed along the Buesaco Fault plane (Fig. 13) at a depth of 11 ± 5 km and its focal mechanism shows a right-lateral strike-slip motion with a reverse component and one nodal plane parallel to the NE strike of the fault (INGEOMINAS, 1995). The Buesaco fault is a Holocene, 29-km-long, structure showing morphological evidence of recent strike-slip motion with uplift of the NW tectonic block (Tibaldi and Romero, 2000). In this area, in addition to the Buesaco Fault, the 13-km-long Aranda Fault (Tibaldi and Romero, 2000) and the 14-km-long Pasto Fault (Rovida and Tibaldi, 2005) are recognised, but it is questionable that all the large seismic events were generated by these relatively short faults, even if the expected earthquake magnitude for the Buesaco Fault is 6.7 (Rovida, 2001).

To the east scattered crustal events with $\mathbf{M} \leq 6$ could be related to segments II and III of the CASF (Fig. 13). A number of earthquakes with lower magnitudes may be referred to

Table 1
Local absolute radiometric dating used as calibration points

Type of deposit	Related volcano	Age BP	Reference
Lava flow	Soche	9.7 ka	Hall and Beate, 1991
Lava flow	Soche	37.22 ± 0.63 ka	Ego et al., 1996
Lahar		8.6 ± 0.06 ka	Ego et al., 1996
Lava dome	Reventador	0.34 Ma	INECEL, 1988
Debris avalanche	Reventador	>30 ka	INECEL, 1988
Debris avalanche	Reventador	18.8 ± 0.5 ka	INECEL, 1988
Pyroclastic	Reventador	19.5 ± 0.2 ka	INECEL, 1988
Fluvio-lacustrine		4 ± 0.1 ka	INECEL, 1988
Fluvio-lacustrine		0.5 ± 0.1 ka	INECEL, 1988

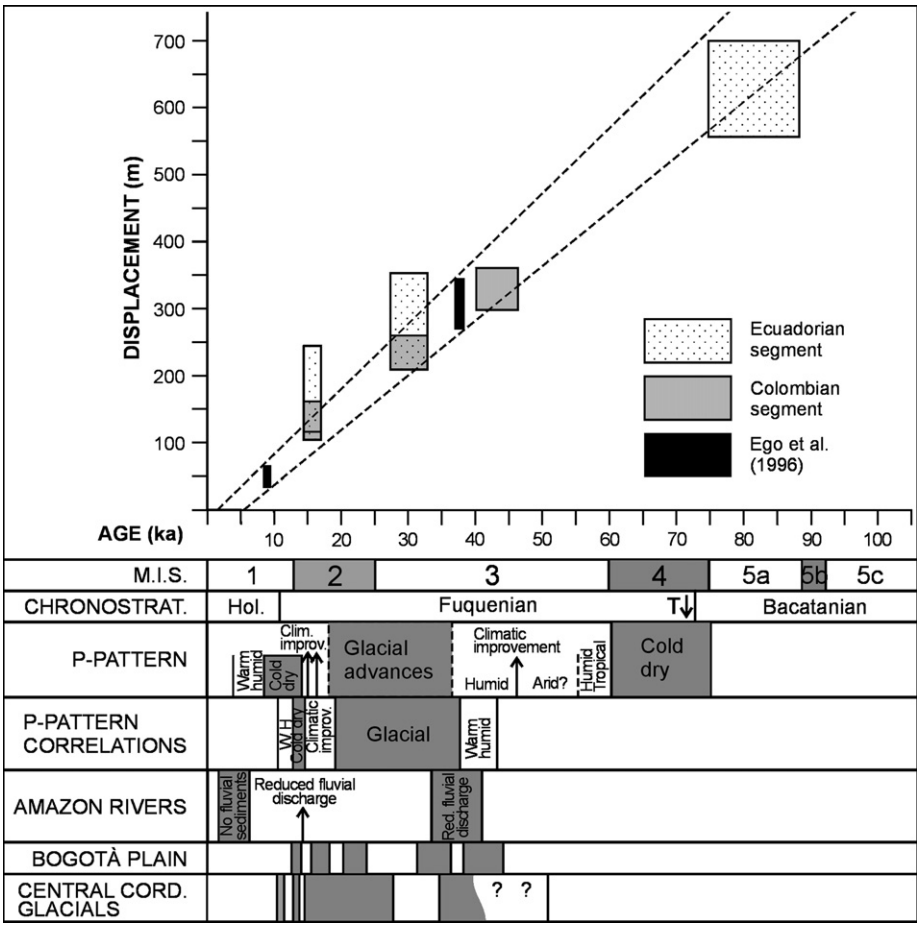

Fig. 12. Graph of right-lateral displacement values of landforms and deposits measured along the CASF versus their inferred ages. Dashed lines represent the slip-rate values obtained by Ego et al. (1996) on the basis of the displacement of the Soche Volcano lava flow. The graph shows a nearly constant slip-rate during the time span 100 ka – Present, and displacement values systematically lower for the Colombian segments of the fault. At the bottom the climatic records used for the age estimation are summarised, M.I.S. (Marine Isotopic Stages) after Martinson et al. (1987), chronostratigraphy after Van der Hammen and Hooghiemstra (1997), P-Pattern and P-Pattern correlations after Iriondo (1999), Amazonian rivers after Dumont et al. (1992), Bogotà plain after Helmens et al. (1997), Central Cordillera glacials after Thouret et al. (1997).

segments V and VI of the CASF. In this area some historical seismicity was also recorded. The strong event ($M_S = 7.0$) of January 1834 near the Sibundoy Valley (Fig. 13) may be related to the CASF (Rovida et al., 2004). At the SW termination of the CASF, a cluster of seismicity of low magnitude ($\mathbf{M} < 4$) is present, together with historical events.

6. Discussion

6.1. Fault age and kinematics

Many elements demonstrate active tectonics along the CASF: the offset of Holocene deposits such as the Soche Volcano lava flow; the offset of recent fossil landforms such as glacial valleys and cirques related to the LGM; the displacement of active river valleys; the presence of faceted spurs and landslides along the fault; and, finally, the pattern of seismicity. Based on the amount of dislocation, hundreds of metres, and on the age of the offset deposits and morphologies, we would argue that the CASF has been active since at least the late Pleistocene.

Our findings of reverse motion along the CASF southern segment in Ecuador are consistent with focal mechanism solutions (Tibaldi, 2005). Both field data and focal mechanisms indicate slip planes dipping at high angle (70–80°) with compressional motion explained as the reactivation of N-S-striking faults within a contractional fan and, farther NE, a restraining bend (Figs. 3 and 5).

The remaining portion of the CASF is, by comparison, characterised by right-lateral strike-slip motion sometimes with a component of relative uplift of the NW tectonic block. Field data and focal mechanism solutions show that the fault plane is nearly vertical or sub-vertical dipping to the WNW. The regional geodynamics are produced by the convergence of the Nazca and South American tectonic plates with nearly E-W subduction of the Nazca Plate. This trench oblique convergence produces NNE-ward escape of the North Andean Block relative to the stable South America plate (Pennington, 1981; Tibaldi and Ferrari, 1992; Kellogg and Vega, 1995) as indicated by intracontinental deformation (Fig. 1) (Schubert, 1980; Tibaldi and Ferrari, 1992; Paris and Romero, 1993;

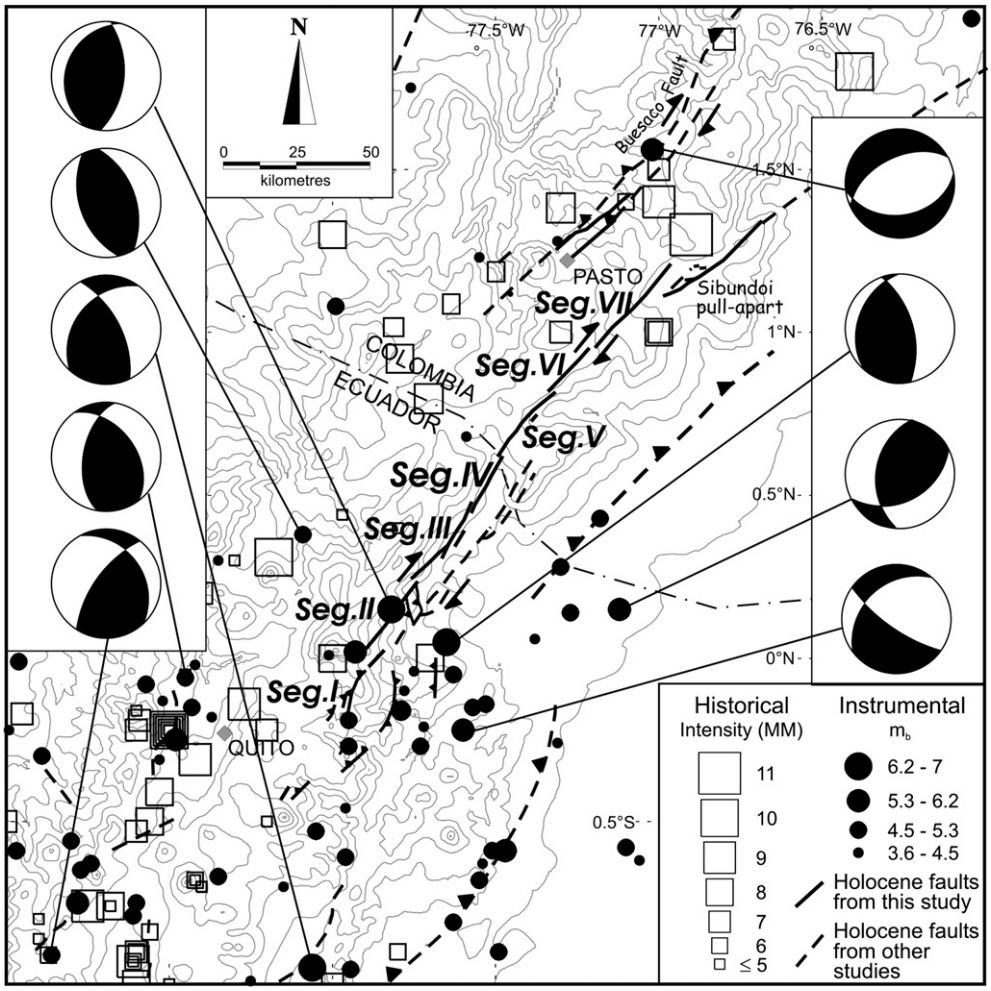

Fig. 13. Map of epicentral locations of seismic events in Southern Colombia and Northern Ecuador and Holocene faults from this study. Instrumental crustal epicentres are from USGS NEIC catalogue (1973–Present), historical epicentres are from CERESIS database (1541–1983). Some focal mechanism solutions from Harvard CMT Catalogue are also shown. Map location is given in Fig. 1.

Chorowicz et al., 1996; INGEOMINAS, 1998) and GPS measurements (Trenkamp et al., 2002). The observed right-lateral strike-slip motion combined with a reverse component along NE- to NNE-striking faults is consistent with this regional tectonic framework and with the E-W-trending compressional stress evidenced by crustal seismicity (Ego et al., 1996) and by field data on recent faults (Romero, 2001).

6.2. Fault slip-rates and deformation in space and time

Measurements along segment I (Fig. 3), show a cumulative short term slip-rate of 4.3 ± 2.2 mm/yr on the three parallel faults. NE of the Cayambe volcano, along segments II, III and IV we calculate a slip-rate of 11.9 ± 0.7 mm/yr for the post-LGM time (short term) and 8.4 ± 0.7 mm/yr for long term time (i.e. post 90 ka BP). To the NE for segments V and VI, we obtained a short term slip-rate of 9.0 ± 3.4 mm/yr and a long term rate of 7.7 ± 0.4 mm/yr.

The computed slip rates are nearly constant for both time spans considered (i.e. post-LGM and post 90 ka BP), except for the short term slip-rate computed for segments II, III and IV that give higher results. Moreover, in any given time-window, the southern segments (mostly in Ecuador) of the CASF have faster motion than the northern segments (in Colombia). This can be explained by the observation that in southern Colombia there is a higher number of parallel to sub-parallel main faults with recent motion, e.g. the Aranda, Pasto and Buesaco faults (INGEOMINAS, 1998; Taboada et al., 2000; Tibaldi and Romero, 2000; Rovida and Tibaldi, 2005) while in northern Ecuador there is just one main late Pleistocene-Holocene deformation system along the Interandean Valley (Tibaldi and Ferrari, 1992; Ego et al., 1996) and in central-southern Ecuador there is only the Pallatanga Fault (Winter et al., 1993). The short-time slip-rates are significantly higher along segments II to IV than along segments V and VI, suggesting that a change from distributed to concentrated deformation happened in recent times in segments II–IV.

Our findings of dominant transcurrent motion of the CASF and the nearly constant slip-rates, also suggest the potential Quaternary activity of the frontal thrust system to the east,

accommodating the E-W component of the convergence between the Nazca and South American plates. In fact, west of the CASF no significant recent/active thrust planes have been recognized, apart from some Quaternary folds and probably associated hidden reverse faults in the Quito and Latacunga areas in the Ecuadorian Interandean Valley (Lavenu et al., 1995; Fiorini et al., 2004). Thus, the E-W contraction should occur on planes with dip-slip reverse motion located to the east, where the frontal faults are the prime candidates (Bès de Berc et al., 2005; Tibaldi, 2005). This situation also implies a very interesting example of Quaternary strain partitioning between strike-slip motion along the cordilleran faults and reverse motion along the parallel faults located at the Andes foreland, similar to that hypothesized by Ferrari and Tibaldi (1992). For these reasons the recent activity of the frontal thrust system should be analysed more in detail, despite the difficult accessibility of the area.

6.3. Implications for seismic hazard

Tens to hundreds of meters of latest Pleistocene-Holocene offset measured along the CASF and the length of the surface fault traces suggest that several seismic events with $\mathbf{M} > 5.5$ may have occurred along this structure, according to the classical surface rupture vs. magnitude model (McCalpin, 1996). Also slip-rate calculations suggest rapid motion along the various fault segments. Some of this motion may occur by creeping, but coseismic displacement should be expected since seismic activity, both instrumental and historical, has been recorded along or close to this fault system. Creep activity has not been demonstrated up to now for the CASF so it is a prime candidate for future shocks of relevant magnitude. We computed the magnitudes of the earthquakes that could be generated by the various fault segments by means of Wells and Coppersmith's (1994) empirical relationship among surface rupture length (SRL) and moment magnitude **M**:

$$Log(SRL) = a + b * \mathbf{M} \quad (1)$$

We applied the appropriate coefficients depending on the observed kinematics, i.e. $a = -3.55 \pm 0.37$ and $b = 0.74 \pm 0.05$ in the case of strike-slip segments and $a = -2.86 \pm 0.55$; $b = 0.63 \pm 0.08$ for reverse faults.

To assess the magnitude of a potential earthquake generated by the CASF, we consider the single observed segments (I to VII) as possible rupture lengths. Based on the close continuity of past surface ruptures, we consider also the possible simultaneous reactivation of segments I, II and III as a unique segment and the simultaneous activation of segments I, II, III, IV, V, VI and VII. The entire structure length (270 km) was considered as the maximum theoretical surface rupture length, applying the generic regression coefficients ($a = -3.22 \pm 0.27$ and $b = 0.69 \pm 0.04$) as the kinematics of the whole structure changes from pure reverse in the south, to pure right-lateral in the central part, to oblique in the north.

Starting from the south, Segment I of the CASF shows three surface rupture traces with pure reverse kinematics and a total rupture length of 15 km. Considering SRL = 15 in Eq. (1) and $a = -2.86 \pm 0.55$, $b = 0.63 \pm 0.08$ (reverse faults) we obtain $\mathbf{M} = 6.4 \pm 0.1$. This result is consistent with the magnitudes of 6.1 and 6.9 (M_S) of the two earthquakes that occurred in this area on March 5, 1987 (USGS, 1987).

Segments II to VII present, respectively, the following surface rupture lengths: 14, 30, 14, 17, 14 and 42 km. Introducing these rupture length values (SRL) in Eq. (1), together with the coefficient a and b valid for strike-slip motion, we obtain $\mathbf{M} = 6.3 \pm 0.1$ for segments II, IV and VI, $\mathbf{M} = 6.8 \pm 0.1$ for segment II, $\mathbf{M} = 6.4 \pm 0.1$ for segment V and $\mathbf{M} = 7.0 \pm 0.1$ for segment VII. The latter is in agreement with the estimated $M_S = 7.0$ of the January 1834 Sibundoy Valley event that has been referred to the CASF (Rovida et al., 2004). For the entire structure length of 270 km as rupture length with $a = -3.22 \pm 0.27$ and $b = 0.69 \pm 0.04$ (general case) we obtain $\mathbf{M} = 8.2 \pm 0.1$. Other cases of potential simultaneous reactivation of different segments of the fault are shown in Table 2.

These results should be carefully considered, as several villages such as La Bonita in Ecuador or Alizales and the

Table 2
Computed moment magnitude (**M**) of potential earthquakes of CASF

Fault segment	Slip type	SRL	a	b	**M**
I	R	15	-2.86 ± 0.55	0.63 ± 0.08	6.4 ± 0.1
II	SS	14	-3.55 ± 0.37	0.74 ± 0.05	6.3 ± 0.1
III	SS	30	-3.55 ± 0.37	0.74 ± 0.05	6.8 ± 0.1
IV	SS	14	-3.55 ± 0.37	0.74 ± 0.05	6.3 ± 0.1
V	SS	17	-3.55 ± 0.37	0.74 ± 0.05	6.4 ± 0.1
VI	SS	14	-3.55 ± 0.37	0.74 ± 0.05	6.3 ± 0.1
VII	SS	42	-3.55 ± 0.37	0.74 ± 0.05	7.0 ± 0.1
I + II	All	29	-3.22 ± 0.27	0.69 ± 0.04	6.8 ± 0.0
I + II + III	All	59	-3.22 ± 0.27	0.69 ± 0.04	7.2 ± 0.0
I + II + III + IV	All	73	-3.22 ± 0.27	0.69 ± 0.04	7.4 ± 0.1
I + II + III + IV + V	All	90	-3.22 ± 0.27	0.69 ± 0.04	7.5 ± 0.1
I + II + III + IV + V + VI	All	104	-3.22 ± 0.27	0.69 ± 0.04	7.6 ± 0.1
I + II + III + IV + V + VI + VII	All	131	-3.22 ± 0.27	0.69 ± 0.04	7.7 ± 0.0
TOTAL	All	270	-3.22 ± 0.27	0.69 ± 0.04	8.2 ± 0.1

Wells and Coppersmith (1994) method. Fault kinematics observed in the field: R = reverse, SS = strike-slip, All = oblique; SRL = surface rupture length; a and b: regression coefficients.

inhabited Sibundoy Valley in Colombia are located along the fault trace. Moreover, the capital of Ecuador, Quito (1,100,000 inhabitants), is located 75 km west of fault Segment I. Otavalo, Ibarra, and Tulcan are located 35–40 km WNW of fault segments II and III. In Colombia, the city of Pasto (400,000 inhabitants), capital of Nariño Department, is 28 km NW of the CASF (segments V and VI). The seismic hazard related to the CASF was estimated as I = VI for Quito (Hibsch et al., 1997) using a slip-rate of 7 mm/yr and a rupture length of 76 km (Chingual Fault, correspondent to segments I, II and III of the CASF).

7. Conclusions

Displacement analysis of the CASF with an estimation of the age for the recent offset of landforms and deposits suggest a latest Pleistocene-Holocene age for its last fault motions. The computed slip-rates for the latest Pleistocene-Holocene fault-segments and the lengths of their surface traces suggest that the CASF was possibly responsible for a number of large earthquakes ($\mathbf{M} > 5.5$) in the past. Unfortunately, the shortness of the historical seismic catalogue of the area (less than 500 years) and the scattered distribution of populated places do not provide an independent record of these earthquakes, underlining the need for further paleoseismological investigations. A recent study (Rovida et al., 2004) related the 1834 Sibundoy ($M_S = 7.0$) and the 1987 Reventador ($M_S = 6.9$) earthquakes to the northern and southern segments of the CASF respectively. The potential moment magnitudes calculated for the different fault segments are medium to high and consistent with the present regional seismicity. These observations and evidence of tectonic activity during the last 90 ka indicate the influence of the CASF on the seismic hazard of the area. Our data also suggest the potential for seismic activity along the frontal thrust system to the east between the Andes and the foreland, accommodating part of the E-W component of convergence between the Nazca and South American plates. Quaternary strain partitioning between strike-slip motion along the cordilleran faults and dip-slip reverse motion along the parallel frontal faults should be studied in more detail.

Acknowledgements

We wish to thank J. Kellogg, D.J. Rust and W. Dunne for their review. Field cooperation with J. Romero Leon and J.A. Osorio in Colombia is acknowledged. The study in Colombia was partly supported by a grant from CNR of Italy and INGEOMINAS of Colombia. Studies in Ecuador were supported by Italian MIUR-FIRB and MIUR-PRIN grants. This study was performed in the framework of the UNESCO-IUGS-IGCP Project n. 455 ‘‘Effects of basement structural and stratigraphic heritages on volcano behaviour and implications for human activities’’ and of the ILP grant ‘‘Tectonic causes of volcano instability’’ coordinated by A. Tibaldi, and the UNESCO-IUGS-IGCP Project n. 508 ‘‘Volcano collapse and fault activity’’, co-led by C. Corazzato. Comments by Y. Branquet on an early version of the manuscript were very helpful.

References

Balseca, W., Ferrari, L., Pasquaré, G., Tibaldi, A., 1993. Geological and Structural Evolution of the Napo Uplift, Sub-Andean Zone, Ecuador. II International Symposium on Andean Geodynamics. ORSTOM, Paris. 163–166.

Barberi, F., Coltelli, M., Ferrara, G., Innocenti, F., Navarro, J.M., Santacroce, R., 1988. Plio-Quaternary volcanism in Ecuador. Geol. Mag. 1, 1–14.

Bès de Berc, S., Soula, J.C., Baby, P., Sourisc, M., Christophoul, F., Rosero, J., 2005. Geomorphic evidence of active deformation and uplift in a modern continental wedge-top-foredeep transition: example of the eastern Ecuadorian Andes. Tectonophysics 399 (1–4), 351–380.

Centro Regional de Sismología para América del Sur (CERESIS), 1985. Catálogo de terremotos para América del Sur. In: Askew, B., Algermissen, S.T. (Eds.) Programa para la mitigación de los efectos de los terremotos en la región andina (Proyecto SISRA). Earthquake Mitigation Program in the Andean Region (Project SISRA), v. 1–9, 269 pp.

Chorowicz, J., Chotin, P., Guillande, R., 1996. The Garzon fault: active southwestern boundary of the Caribbean plate in Colombia. Geol. Rundsch. 85, 172–179.

Direcciòn General de Geologìa y Minas (DGGM), 1986. Mapa geologico ‘‘S. Gabriel’’, escala 1:100.000. Quito, Ecuador.

Dumont, J., Garcia, F., Fournier, M., 1992. In: Orlieb, L., Macharé, J. (Eds.), Registros de cambios climaticos por los depositos y morfologias fluviales en la Amazonia Occidental. Paleo-ENSO Records Int. Symp., Ext. Abs. ORSTROM-CONCYTEC, Lima, pp. 87–92.

Dziewonski, A.M., Ekstrom, G., Woodhouse, J.H., Zwart, G., 1988. Centroid moment tensor solutions for January–March, 1987. Phys. Earth Planet. Inter. 50, 116–126.

Ego, F., Sébrier, M., Lavenu, A., Yepes, H., Egues, A., 1996. Quaternary state of stress in the Northern Andes and the restraining bend model for the Ecuadorian Andes. Tectonophysics 259, 101–116.

Escallon, J., Pinzon, J., Gomez, I., 1993. Actualizacion de la informacion sismica de Colombia, Internal Report of Red Sismologica Nacional de Colombia, Inst. Nac. Invest. Geol. Min., Bogotá, Colombia, 98 pp.

Espinosa, A., 1994. Contribuciones al catalogo colombiano de sismicitad historica. Rev. Colomb. Inst. Nac. Invest. Geol. Min. 4, 77–82.

Feininger, T., Bristow, C.R., 1980. Cretaceous and Paleogene geologic history of coastal Ecuador. Geol. Rundschau. 69, 849–874.

Ferrari, L., Tibaldi, A., 1989. Seismotectonics of North-Eastern Ecuadorian Andes. Annales Geophisicae, special issue on EGS XIV General Assembly, 39, (abstract).

Ferrari, L., Tibaldi, A., 1992. Recent and active tectonics of the north-eastern Ecuadorian Andes. J. Geodyn. 15, 39–58.

Fiorini, E., Garcia, M., Tibaldi, A., Zonno, G., 2004. Preliminary Results for Seismic Hazard Assessment of the Region Surrounding the Cotopaxi Volcano, Ecuador. ESC XXIV General Assembly, Postdam, Germany, September 12–17, 2004, abstract, page 50.

Gaudemer, Y., Tapponnier, P., Turcotte, D.L., 1989. River offsets and active strike-slip faults. Ann. Tecton. 3, 55–76.

Gonzalez, H., Nuñez, A., Paris, G., 1988. Mapa geológico de Colombia – Memoria explicativa. Inst. Nac. Invest. Geol. Min., Bogotà.

Groppelli, G., Tibaldi, A., 1999. Control of rock rheology on deformation style and slip-rate along the active Pernicana fault, Mt. Etna, Italy. Tectonophysics 305, 521–537.

Hall, L.M., Beate, B., 1991. El volcanismo plio-cuaternario en los Andes del Ecuador. Estudios Geogr. 4, 5–17.

Helmens, K.F., Rutter, N.W., Kuhry, P., 1997. Glacier fluctuations in the Eastern Andes of Colombia (South America) during the last 45,000 radiocarbon years. Quat. Int. 38/39, 39–48.

Henderson, W.G., 1979. Cretaceous to Eocene volcanic arc activity in the Andes of northern Ecuador. J. Geol. Soc. London 136, 367–378.

Heusser, C.J., 1974. Vegetation and climate of the Southern Chilean Lake District during and since the last interglaciation. Quat. Res. 4, 290–315.

Hibsch, C., Alvarado, A., Yepes, H., Perez, V.H., Sébrier, M., 1997. Holocene liquefaction and soft-sediment deformation in Quito (Ecuador): a paleoseismic history recorded in lacustrine sediments. J. Geodyn. 1-4, 259–280.

Instituto de Investigaciones y Informacion Geocientifica Minero Ambiental y Nuclear (INGEOMINAS), 1988. Mapa geologico de Colombia, 1:500,000 scale, Bogotá, Colombia.

Instituto de Investigaciones y Informacion Geocientifica Minero Ambiental y Nuclear (INGEOMINAS), 1995. El sismo de Pasto (Nariño) del 4 de Marzo de 1995. Bol. de Sismos 1, 63–70.

Instituto de Investigaciones y Informacion Geocientifica Minero Ambiental y Nuclear (INGEOMINAS), 1998. Base de datos de fallas activas de Colombia – Recopilacion bibliografica. Proyecto de amenanza sismica en el Territorio colombiano (C98R04), Bogotà, Colombia.

Instituto Nacional de Electrificacion (INECEL), 1988. Estudio volcanologico de "El Reventador". Quito, Ecuador, 117 pp.

Iriondo, M., 1999. Climatic changes in the South American plains: record of a continent scale oscillation. Quat. Int. 57/58, 93–112.

Kellogg, J.N., Vega, V., 1995. Tectonic development of Panama, Costa Rica, and the Colombian Andes: constraints from Global Positioning System geodetic studies and gravity. In: Mann, P. (Ed.), Geologic and Tectonic Development of the Caribbean Plate Boundary in Southern Central America. Geol. Soc. Am. Spec. Pub. 295, pp. 75–90.

Lavenu, A., Winter, T., Devila, F., 1995. A Pliocene-Quaternary compressional basin in the Interandean Depression, Central Ecuador. Geophys. J. Int. 121, 279–300.

Lebrat, M., Mègard, F., Dupuy, C., Dostal, J., 1987. Geochemistry and tectonic setting of pre-collision Cretaceous and Paleogene volcanic rocks of Ecuador. Geol. Soc. Am. Bull. 99, 569–578.

Litherland, M., Aspden, J.A., 1992. Terrane-boundary reactivation: a control on the evolution of the Northern Andes. J. South Am. Earth Sci. 1, 71–76.

Martinson, D.G., Pisias, N.G., Hays, J.D., Imbrie, J., Moore, T.C., Shackleton, N.J., 1987. Age dating and the orbital theory of the ice ages: development of a high-resolution 0 to 300,000-year chronostratigraphy. Quat. Res. 27, 1–29.

McCalpin, J.P. (Ed.), 1996. Paleoseismology. Academic Press, San Diego, p. 583.

McClay, K.R., 1992. Glossary of Thrust Tectonics Terms. In: McClay, K.R. (Ed.), Thrust Tectonics. Chapman & Hall, p. 447.

Montgomery, D.R., Balco, G., Willet, S.D., 2001. Climate, tectonics, and the morphology of the Andes. Geology 29 (7), 579–582.

Paris, G., Romero, J., 1993. Fallas activas en Colombia. Bol. Geol. Colomb. Inst. Nac. Invest. Geol. Min, 3–25.

Pasquaré, G., Tibaldi, A., Ferrari, L., 1990. Relationships between plate convergence and tectonic evolution of the Ecuadorian active Thrust Belt. In: Critical Aspects of Plate Tectonic Theory. Theophrastus Publications, Athens. 365–387.

Pennington, W.D., 1981. Subduction of the Eastern Panama Basin and seismotectonics of North Western South America. J. Geophys. Res. 86, 10753–10770.

Ramirez, J.E., 1975. Historia de los terremotos en Colombia. Report Inst. Geogr. A. Codazzi, Bogotá, Colombia, 250 pp.

Romero, J.A., 2001. Sismotectonica de la Region del Volcan Galeras, Colombia. PhD Thesis, Universitad de Barcelona – CSIC, 230 pp.

Roperch, P., Mègard, F., Laj, C., Mourier, T., Clube, T.M., Noblet, C., 1987. Rotated oceanic blocks in western Ecuador. Geophys. Res. Lett. 14, 558–561.

Rovida, A., 2001. Neotettonica in aree urbane: l'esempio di Pasto (Colombia meridionale). MSc Thesis, Univ. Milano-Bicocca.

Rovida, A., Tibaldi, A., 2005. Propagation of strike-slip faults across Holocene volcano-sedimentary deposits, town of Pasto, Colombia. J. Struct. Geol. 27, 1838–1855.

Rovida, A., Gomez Capera, A.A., Leschiutta, I., 2004. An integrated geological, macroseismic and seismological source model for the 1834 Southern Colombia and 1987 Northern Ecuador earthquakes. Geophysical Research Abstracts, vol. 6, EGU General Assembly.

Schubert, C., 1980. Late Cenozoic pull-apart basins. Bocono fault zone, Venezuelan Andes. J. Struct. Geol. 2 (4), 463–468.

Strom, A., 1999. Sources of uncertainty in the course of past earthquakes parameters assessment. J. Geology 13-14, 292–295.

Taboada, A., Rivera, L.A., Fuenzalida, A., Cisternas, A., Hervé, P., Bijwaard, H., Olaya, J., Rivera, C., 2000. Geodynamics of the northern Andes: subductions and intracontinental deformation (Colombia). Tectonics 19, 787–813.

Thouret, J.C., Van Der Hammen, T., Salomons, B., Juvigné, E., 1997. Late Quaternary glacial stades in the Cordillera Central, Colombia, based on glacial geomorphology, tephra-soil stratigraphy, palynology, and radiocarbon dating. J. Quat. Sci. 12, 347–369.

Tibaldi, A., 1998. Effects of topography on surface fault geometry and kinematics: examples from the Alps, Italy, and Tien Shan, Kazakstan. Geomorphology 2-3, 225–243.

Tibaldi, A., 2005. Volcanism in compressional tectonic settings: Is it possible? Geophys. Res. Letts. 32, doi:10.1029/2004GL021798. L06309.

Tibaldi, A., Ferrari, L., 1992. Latest Pleistocene-Holocene tectonics of the Ecuadorian Andes. Tectonophysics 205, 109–125.

Tibaldi, A., Romero, J., 2000. Morphometry of Late Pleistocene-Holocene faulting and volcano-tectonic relationship in the southern Andes of Colombia. Tectonics 4, 358–377.

Trenkamp, R., Kellogg, J.N., Freymuller, J.T., Mora, H.P., 2002. Wide plate margin deformation, south Central America and northwestern South America, CASA GPS observations. J. South Am. Earth. Sci. 15, 157–171.

United States Geological Survey (USGS), 1987. Preliminary Determination of Epicenters (PDE). Monthly Listing, March 1987. U.S. Dept. of the Interior.

Van der Hammen, T., Hooghiemstra, H., 1997. Chronostratigraphy and correlation of the Pliocene and Quaternary of Colombia. Quat. Int. 40, 81–91.

Velandia, F., Acosta, J., Terraza, R., Villegas, H., 2005. The current tectonic motion of the Northern Andes along the Algeciras Fault System in SW Colombia. Tectonophysics 399 (1–4), 313–329.

Wallace, R.E., 1968. Notes on stream channels offset by the San Andreas fault, southern Coast ranges, California. In: Dickinson, W.R., Grantz, A. (Eds.), Geological Problems of the San Andreas Fault System. Stanford Univ. Publ. Geol. Sci., 11, pp. 6–21.

Wallrabe-Adams, H.J., 1990. Petrology and geotectonic development of the Western Ecuadorian Andes: the Basic Igneous Complex. Tectonophysics 185, 163–182.

Wells, D.L., Coppersmith, K.J., 1994. New empirical relationships among magnitude, rupture length, rupture width, rupture area, and surface displacement. Bull. Seism. Soc. Am. 84 (4), 974–1002.

Winter, T., Avouac, J.P., Lavenu, A., 1993. Late Quaternary kinematics of the Pallatanga strike-slip fault (Central Ecuador) from topographic measurements of displaced morphologic features. Geophys. J. Int. 115, 905–920.

Woodcock, N.H., Fischer, M., 1986. Strike-slip duplexes. J. Struct. Geol. 7, 725–735.